

The footprint of nuclear saturation properties on the neutron star f mode oscillation frequencies: a machine learning approach

Deepak Kumar^{1,*}, Tuhin Malik^{2,†} and Hiranmaya Mishra^{3,‡}

¹*Department of Physics, Indian Institute of Science Education and Research, Bhopal, 462 066, India*

²*CFisUC, Department of Physics, University of Coimbra, PT 3004-516 Coimbra, Portugal and*

³*School of Physics, National Institute of Science Education and Research,
An OCC of Homi Bhabha National Institute, Jatni - 752050, India*

We investigate the intricate relationships between the non-radial f mode oscillation frequencies of neutron stars (NSs) and the corresponding nuclear matter equation of state (EOS) using a machine learning (ML) approach within the ambit of the relativistic mean field (RMF) framework for nuclear matter. With two distinct parameterizations of the Walecka model, namely, (1) with non-linear self interactions of the scalar field (NL) and, (2) a density dependent Bayesian model (DDB), we perform a thorough examination of the f mode frequency in relation to various nuclear saturation properties. The correlations between the f mode frequencies and nuclear saturation properties reveal, through various analytical and ML methods, the complex nature of NSs and their potential as the cosmic laboratory for studying extreme states of matter. A principal component analysis (PCA) has been performed using mixed datasets from DDB and NL models to discriminate the relative importance of the different components of the EOS on the f mode frequencies. Additionally, a *Random forest feature importance* analysis also elucidates the distinct roles of these properties in determining the f mode frequency across a spectrum of NS masses. Our findings are further supported by symbolic regression searches, yielding high-accuracy relations with strong Pearson coefficients and minimal errors. These relations suggest new methodologies for probing NS core characteristics, such as energy density, pressure, and speed of sound from observations of non-radial f mode oscillations of NSs.

I. INTRODUCTION

The most fascinating neutron rich astrophysical compact objects, neutron star (NS)s, are the second densest objects in the universe after black holes, born from a supernovae explosion and are observed as pulsars. They provide us a system to investigate the behaviour of strongly interacting cold baryonic matter under extreme densities which are not accessible to a accelerator experiments in the laboratories on the earth at present [1]. On the other hand, in recent years, the observation of compact stars have reached unprecedented levels of precision providing very useful insight to constraints the properties of super dense matter. One of the strongest constraint comes from the observations of high mass pulsars PSR J0740+6620 which has pushed the maximum mass to $2.08 \pm 0.07 M_{\odot}$ [2]. Another constraint is provided by the radius estimation from low mass binaries and objects with photospheric radius expansion busts, which suggest small NS radii, but it has much larger uncertainties than the mass measurements [3]. The other concern measurement in this context is the simultaneous mass measurement for PSR J0030+7451 [4, 5] and J0740+6620 [6, 7] extracted from the X-rays observations using Neutron Star Interior Composition Explorer (NICER) instrument. Furthermore, the detection of gravitational

wave (GW)s from binary NS merger GW170817 that provides an estimate of tidal deformability that can further yield the constraints on the radii of the individual components [8, 9].

Determining the composition of matter inside the core of neutron stars (NSs) is challenging due to significant uncertainties in observing their properties, such as radius, in the electromagnetic spectrum [10–13]. The determination of the composition of NSs, which pertains to the behavior of matter that strongly interacts under extreme conditions, is anticipated to be achieved by investigating asteroseismology in isolated NSs. This topic has been extensively explored and deliberated in several scholarly works [14–19]. In addition to the mass-radius and the tidal deformation constraining the equation of state (EOS) of dense matter, oscillation frequencies of NSs are strongly depend on the properties of the matter constituting the interior of NSs [20–24]. Theoretically the non-radial oscillations can be studied in the frame work of general relativity where the fluid perturbations can be decomposed into the spherical harmonics. The even parity of harmonics corresponds to the polar deformation which can further be classified into different kinds of modes depending upon the restoring forces acting on the fluid when it displaced from its equilibrium position. They are the fundamental (f modes), pressure (p modes), gravity (g modes) and a branch of space-time modes - the polar (w modes). The frequency of g mode is lower than that of the p modes while f mode frequencies lie in between them. The focus of the present investigation is on the f modes [25]. These oscillation modes couples to GWs and hence it is expected that the fea-

*Electronic address: dpqraja02@gmail.com

†Electronic address: tuhin.malik@uc.pt

‡Electronic address: hiranmaya@niser.ac.in

tures of GWs originating of such QNMs can be verified by the advance GW detectors like Einstein telescope in near future [26].

One of the important development in this context has been to relate the frequencies of f modes to the NSs global structural properties which can constrain the nuclear matter EOS. On the other hand the present investigation aims to study the constraints on the features of the nuclear matter imposed by the f mode oscillations of the NSs. In particular, it will be investigated the relative contributions of different individual nuclear matter saturation properties to the f mode oscillations of different NSs masses through the principal component analysis (PCA) [27] and the machine learning (ML) approaches. In this context, it may be pointed out that such a correlation study has been attempted recently to obtain universal relations of neutron star features of EOS of dense matter [22, 28].

It may be noted that recently, ML techniques, in particular, use of neural network and deep learning have been applied to explore the properties of NS matter as well as in the regimes valid for perturbative quantum chromodynamics (QCD) [29–34]. Bayesian Neural Networks (BNNs) have been employed to determine the internal composition of neutron stars (NSs) by analyzing simulated observations of their radius and tidal deformability [35]. In addition to conventional machine learning models, feed-forward artificial neural networks were employed to extrapolate the separation energy of hypernuclei [36]. Furthermore, studies have demonstrated that neural networks are capable of dealing with intricate non-linear connections between observables and the fundamental physics in the context of reconstructing the equation of state (EoS) for dense matter based on observations of mass-radius (M-R) and other parameters of neutron stars (NSs) [29, 37]. We use here ML, in particular, symbolic regression [38, 39] to uncover the hidden relations between the nuclear matter parameters and the various stellar properties of NSs.

Our analysis uses two sets of relativistic mean field (RMF) EOSs: one having non-linear interaction terms for the meson fields while the other having density dependent meson couplings which are constrained by the nuclear matter saturation properties at saturation density. In Ref. [28], a statistical data analysis using various correlation measures was used to find out universal relation with multiple variable of NSs. On the other hand, the present analysis complements such an investigation using the techniques of artificial intelligence (AI) with symbolic regression to examine universal relations. In addition we also calculate correlations of different saturation properties of nuclear EOS with the various NS attributes like mass (M), radius (R), tidal deformability (Λ) and non-radial oscillations.

The following is the organization of the article. In section II, we discuss the formalism regarding the nuclear matter EOS in different models. The non-radial oscillation equations of NSs will be discussed in section III.

The section IV covers the sampling processes and data set used in symbolic regression and its importance in our study. In the V section, we present the results of our analyses along with relevant figures and tables, followed by a discussion. Finally, the VI section offers a concluding summary that highlights the main takeaways from our research. We use natural units here where $\hbar = c = G = 1$.

II. FORMALISM

A. Equation of state for nuclear matter

We discuss briefly the general RMF framework to construct EOS of the neutron star matter (NSM). In this framework, the interactions among the baryons are realized through the exchange of mesons. We confine our analysis for the NSM constituting of baryons (neutron and proton) and leptons (electron and muon). The scalar σ mesons create a strong attractive interactions, the vector ω mesons, on the other hand, are responsible for the repulsive short range interactions. The neutrons and protons do only differ in terms of their isospin projections. The isovector ρ mesons are included to distinguish between baryons [40–43]. The Lagrangian including baryons as the constituents of nuclear matter and mesons as the carriers of the interactions is given as [25, 44, 45]

$$\mathcal{L} = \sum_b \mathcal{L}_b + \mathcal{L}_l + \mathcal{L}_{\text{int}}, \quad (1)$$

where,

$$\mathcal{L}_b = \sum_b \bar{\Psi}_b (i\gamma_\mu \partial^\mu - q_b \gamma_\mu A^\mu - m_b + g_\sigma \sigma - g_\omega \gamma_\mu \omega^\mu - g_\rho \gamma_\mu \vec{I}_b \vec{\rho}^\mu) \Psi_b, \quad (2)$$

$$\mathcal{L}_l = \bar{\psi}_l (i\gamma_\mu \partial^\mu - q_l \gamma_\mu A^\mu - m_l) \psi_l, \quad (3)$$

$$\begin{aligned} \mathcal{L}_{\text{int}} = & \frac{1}{2} \partial_\mu \sigma \partial^\mu \sigma - \frac{1}{2} m_\sigma^2 \sigma^2 - V(\sigma) - \frac{1}{4} \Omega^{\mu\nu} \Omega_{\mu\nu} \\ & + \frac{1}{2} m_\omega^2 \omega_\mu \omega^\mu, \\ & - \frac{1}{4} \vec{R}^{\mu\nu} \vec{R}_{\mu\nu} + \frac{1}{2} m_\rho^2 \vec{\rho}_\mu \vec{\rho}^\mu - \frac{1}{4} F^{\mu\nu} F_{\mu\nu}, \end{aligned} \quad (4)$$

and,

$$V(\sigma) = \frac{\kappa}{3!} (g_{\sigma N} \sigma)^3 + \frac{\lambda}{4!} (g_{\sigma N} \sigma)^4. \quad (5)$$

Where $\Omega_{\mu\nu} = \partial_\mu \omega_\nu - \partial_\nu \omega_\mu$, $\vec{R}_{\mu\nu} = \partial_\mu \vec{\rho}_\nu - \partial_\nu \vec{\rho}_\mu$ and $F_{\mu\nu} = \partial_\mu A_\nu - \partial_\nu A_\mu$ are the mesonic and electromagnetic field strength tensors. \vec{I}_b denotes the isospin operator. The Ψ_b and ψ_l are baryon and lepton doublets. The σ , ω and ρ meson fields are denoted by σ , ω and ρ and their masses are m_σ , m_ω and m_ρ , respectively. The parameters m_b and m_l denote the vacuum masses of baryons and leptons. The g_σ , g_ω and g_ρ are the scalar, the vector and the isovector meson-baryon coupling constants respectively. In RMF, one replaces the meson fields by their

expectation values which then act as the classical fields in which baryons move *i.e.* $\langle \sigma \rangle = \sigma_0$, $\langle \omega_\mu \rangle = \omega_0 \delta_{\mu 0}$, $\langle \rho_\mu^a \rangle = \delta_{\mu 0} \delta_3^a \rho_3^0$. The mesonic equations of motion can be found by the Euler-Lagrange equations for the meson fields as derived in [25] using the Lagrangian Eq. (1). The expectation value of σ field redefines the masses while the expectation values of ω and ρ redefine the chemical potentials of the particles. The effective mass and effective chemical potentials are given as follows [25]

$$\begin{aligned} m_b^* &= m_b - g_\sigma \sigma_0, \\ \tilde{\mu}_b &= \mu_b - g_\omega \omega_0 - g_\rho I_{3b} \rho_3^0, \end{aligned} \quad (6)$$

where μ_b is the chemical potential of a baryon, b . We later define it in terms of baryon and electric chemical potentials. The total energy density (ϵ) within the RMF model is given as follows,

$$\begin{aligned} \epsilon &= \frac{m_b^{*4}}{\pi^2} \sum_{b=n,p} H(k_{Fb}/m_b^*) + \frac{1}{2} m_\sigma^2 \sigma_0^2 + V(\sigma_0) \\ &+ \frac{1}{2} m_\omega^2 \omega_0^2 + \frac{1}{2} m_\rho^2 \rho_3^0{}^2, \end{aligned} \quad (8)$$

where k_{Fb} is the Fermi momenta of a baryon and the function $H(z)$ is given as [25]

$$H(z) = \frac{1}{8} \left[z \sqrt{1+z^2} (1+2z^2) - \sinh^{-1} z \right], \quad (9)$$

The pressure (p) can be found using the thermodynamic relation as

$$p = \sum_{b=n,p} \mu_b n_b - \epsilon, \quad (10)$$

where $n_b = \frac{\gamma k_{Fb}^3}{6\pi^2}$, (γ is the degeneracy factor), is the baryon number density of a baryon, b . The Fermi momenta (k_{Fb}) is defined as $k_{Fb} = \sqrt{\tilde{\mu}_b^2 - m_b^{*2}}$ when $\tilde{\mu}_b > m_b^*$ and $k_{Fb} = 0$ otherwise.

We have discussed RMF model with the non linear (NL) interaction terms in Lagrangian Eq. (1) as presented in Refs. [25, 44, 45], which is consistent with the phenomenology of saturation properties of nuclear matter as well as the GWs data regarding tidal deformation [46]. In case of density depended couplings with Bayesian analysis (DDB) model, the meson to baryon couplings are density dependent rather constant in NL model and defined as

$$g_\sigma = g_{\sigma 0} e^{-(x^{a_\sigma} - 1)}, \quad (11)$$

$$g_\omega = g_{\omega 0} e^{-(x^{a_\omega} - 1)}, \quad (12)$$

$$g_\rho = g_{\rho 0} e^{-a_\rho(x-1)}, \quad (13)$$

where, $x = n_B/n_0$, the nuclear saturation density n_0 , and g_{b0} , a_b , ($b = \sigma, \omega, \rho$) are the DDB model parameters. In DDB parameterisation, the cubic and quartic terms in Eq. (1) are taken to be zero so that $V(\sigma) = 0$ and the effective baryon chemical potential as in Eq. (7) gets redefine as

$$\tilde{\mu}_b = \mu_b - g_\omega \omega_0 - g_\rho I_{3b} \rho_3^0 - \Sigma^r, \quad (14)$$

where, Σ^r is the ‘‘rearrangement term’’ which is given as [47]

$$\Sigma^r = \sum_{b=n,p} \left\{ -\frac{\partial g_\sigma}{\partial n_B} \sigma_0 n_b^s + \frac{\partial g_\omega}{\partial n_B} \omega_0 n_b + \frac{\partial g_\rho}{\partial n_B} \rho_3^0 I_{3i} n_b \right\} \quad (15)$$

where $n_B = \sum_b n_b$ is the total baryon number density. The scalar baryon number density of a baryon, b , (n_b^s) is given as [25]

$$n_b^s = \frac{\gamma}{(2\pi)^3} \int_0^{k_{Fb}} \frac{m_b^*}{\sqrt{k^2 + m_b^{*2}}} d^3 k. \quad (16)$$

The matter inside the core is in β -equilibrium which decides the chemical potentials and the baryon number densities of the constituents of NSM. The following equations are the relations the β -equilibrium and charge neutrality,

$$\mu_b = \mu_B + q_b \mu_E, \quad (17)$$

$$\sum_{b=n,p,l} n_b q_b = 0, \quad (18)$$

where, μ_B and μ_E are the baryon and electric chemical potentials and q_b is the charge of the b^{th} particle. The leptonic contribution to the energy density, Eq. (8), and pressure, Eq. (10) is also added to obtain the final definition of EOSs.

Once an EOS model is available, it becomes possible to calculate different nuclear saturation properties. These properties are characterized by expansion coefficients around the saturation density for both symmetric and asymmetric nuclear matter [48].

To generate the EOS datasets, we use the Bayesian analysis, as described in Refs. [22, 49–53], which enables us to carry out a detailed statistical analysis of the parameters of a model for a given set of fit data [54–57]. For a good approximation of the coupling parameters, the EOS of nuclear matter is decomposed into two parts (i) the EOS for symmetric nuclear matter $\epsilon(n_B, 0)$ and (ii) a term involving the symmetry energy coefficient $S(n_B)$ and isospin asymmetry parameter δ as, where $\delta = \frac{n_n - n_p}{n_B}$,

$$\epsilon(n_B, \delta) \simeq \epsilon(n_B, 0) + S(n_B) \delta^2, \quad (19)$$

We can recast EOSs in terms of various bulk nuclear matter properties of order j at saturation density, n_0 : (i) for the symmetric nuclear matter, the energy per nucleon $\epsilon_0 = \epsilon(n_0, 0)$ ($j = 0$), the incompressibility coefficient K_0 ($j = 2$), the skewness Q_0 ($j = 3$), and the kurtosis Z_0 ($j = 4$), respectively as given in Ref. [49]

$$X_0^{(j)} = 3^j n_0^j \left(\frac{\partial^j \epsilon(n_B, 0)}{\partial n_B^j} \right)_{n_0} : \quad j = 2, 3, 4; \quad (20)$$

(ii) for the symmetry energy, the symmetry energy at saturation density $J_{\text{sym},0}$ ($j = 0$),

$$J_{\text{sym},0} = S(n_0), \quad S(n_B) = \frac{1}{2} \left(\frac{\partial^2 \epsilon(n_B, \delta)}{\partial \delta^2} \right)_{\delta=0}, \quad (21)$$

the slope $L_{\text{sym},0}$ ($j = 1$), the curvature $K_{\text{sym},0}$ ($j = 2$), the skewness $Q_{\text{sym},0}$ ($j = 3$) and the kurtosis $Z_{\text{sym},0}$ ($j = 4$) are defined as

$$X_{\text{sym},0}^{(j)} = 3^j n_0^j \left(\frac{\partial^j S(n_B)}{\partial n_B^j} \right)_{n_0} : j = 1, 2, 3, 4. \quad (22)$$

In the Bayesian analysis, the basic rules of probabilistic inference are to update the probability for a hypothesis under the available evidence according to Bayes theorem. The posterior distributions of the model parameters θ in Bayes theorem can be written as [49]

$$P(\theta|D) = \frac{\mathcal{L}(D|\theta)P(\theta)}{\mathcal{Z}}, \quad (23)$$

where θ and D denote the set of model parameters and the available data in terms of nuclear saturation properties etc. The $P(\theta)$, \mathcal{Z} and $P(\theta|D)$ are the prior, the evidence and the joint posterior distribution of the model parameters respectively. The type of prior can be chosen with the preliminary knowledge of the model parameters [49]. The $\mathcal{L}(D|\theta)$ is the likelihood function.

We generate samples of around 18000 final models for each DDB [49] and NL [58] EOSs which satisfy the nuclear matter properties, the pure neutron matter (PNM) EOS calculated from a precise N³LO calculation in chiral effective field theory (chiEFT) and the lowest bound of NS observational maximum mass.

III. NON-RADIAL FLUID OSCILLATION MODES OF COMPACT STARS

In this section, we outline the equations governing the oscillations of NS fluid comprising NSM. We start with the most general metric for a spherically symmetric space-time [25, 59]

$$ds^2 = e^{2\nu} dt^2 - e^{2\lambda} dr^2 - r^2(d\theta^2 + \sin^2\theta d\phi^2), \quad (24)$$

where, ν and λ are the metric functions. The mass function, $m(r)$, in the favor of $\lambda(r)$ is defined as, $\lambda(r) = -\frac{1}{2} \log(1 - \frac{2m}{r})$. From the line element, given in Eq. (24), one can obtain the structure of spherically symmetric compact objects by solving the Tolmann-Openheimer-Volkoff (TOV) equations [25]

$$p' = -(\epsilon + p)\nu', \quad (25)$$

$$m' = 4\pi r^2 \epsilon, \quad (26)$$

$$\nu' = \frac{m + 4\pi r^3 p}{r(r - 2m)}. \quad (27)$$

where prime denotes a derivative with respect to r and, $\epsilon(r)$ and $p(r)$ are energy density and pressure at radial distance r respectively. The $m(r)$ is the mass of compact star enclosed within a radius r . These TOV equations can be integrated from the center ($r = 0$) to the surface

($r = R$) for a given EOS with the following boundary conditions, [25]

$$m(0) = 0, p(0) = p_c, p(R) = 0, \text{ and } e^{2\nu(R)} = 1 - \frac{2M}{R},$$

where p_c is the pressure at the centre of a NS. The radius R is defined as the radial distance from the centre to the surface where pressure vanishes while integrating out Eqs. (25, 26 and 27) from $r = 0$ to $r = R$. The total mass of the star is given by $M = m(R)$.

By linearising the relativistic Euler equation [60] for perfect fluid in perturbation, one can find the pulsating equations which govern oscillations in the fluid as follows [25, 61, 62]

$$Q' = \frac{1}{c_s^2} [\omega^2 r^2 e^{\lambda-2\nu} Z + \nu' Q] - l(l+1)e^\lambda Z, \quad (28)$$

$$Z' = 2\nu' Z - e^\lambda \frac{Q}{r^2} \quad (29)$$

These two coupled first order differential equations, Eqs. (28 and 29), for the perturbing functions $Q(r)$ and $Z(r)$ are to be solved with appropriate boundary conditions at the center and the surface along with the TOV equations, Eqn. (25 and 26). Near the center of a NS, the behaviors of the functions $Q(r)$ and $Z(r)$ are given by [25, 61, 62]

$$Q(r) = Cr^{l+1} \quad \text{and} \quad Z(r) = -Cr^l/l \quad (30)$$

where, C is an arbitrary constant and l is an order of the oscillations. We, here, consider only quadruple ($l = 2$) modes. The other boundary condition is the vanishing of the Lagrangian perturbation pressure, i.e. $\Delta p = 0$ which results the following equation at the surface, [25, 61, 62]

$$\omega^2 r^2 e^{\lambda-2\nu} Z + \nu' Q \Big|_{r=R} = 0. \quad (31)$$

IV. ANALYSIS

A. Dataset

This analysis utilizes two datasets, DDB and NL. The former focuses on density-dependent coupling while the later concerns with constant meson coupling with non-linear meson interactions. Each EOS set with approximately 18,000 samples of parameter sets is the entire posterior generated through a Bayesian inference approach. Such a set is used with minimal constraints applied on nuclear saturation properties, low-density pure neutron matter EOS constrained by chiEFT calculations, and NS mass greater than $2M_\odot$. We, then, construct a tabulated data set from both EOS sets, which includes columns/features such as binding energy per nucleon (ϵ_0), incompressibility (K_0), skewness parameter (Q_0), kurtosis parameter (Z_0), symmetry energy coefficient ($J_{\text{sym},0}$), slope parameter ($L_{\text{sym},0}$), curvature parameter ($K_{\text{sym},0}$), 3rd derivative of symmetry energy

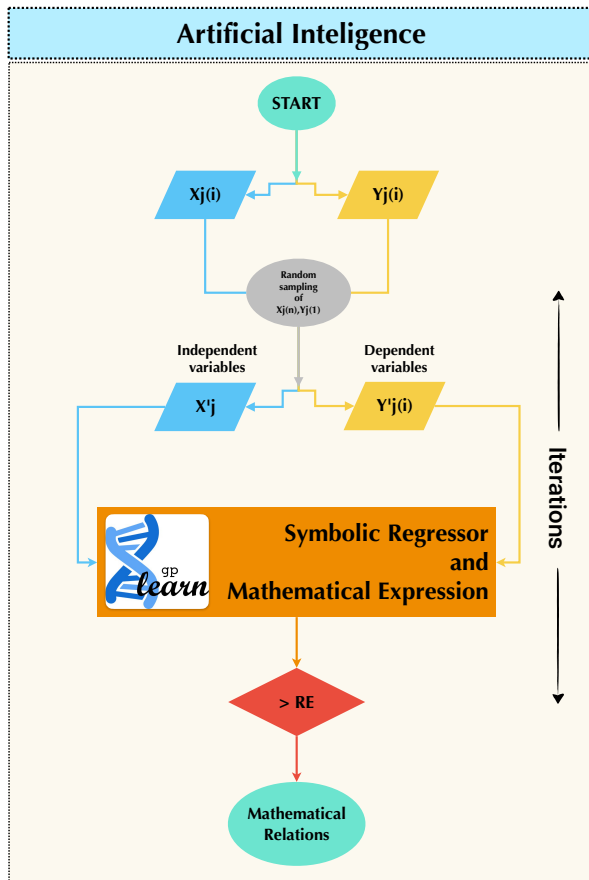


FIG. 1: Schematic representation of the work flow used in our work with the GPlearn algorithm to perform symbolic regression (see the text for more details).

($Q_{\text{sym},0}$), and 4th derivative of symmetry energy ($Z_{\text{sym},0}$) at saturation density ρ_0 as well as the squares of sound speed, central baryon density (ρ_c) and a non-radial oscillation frequency of the f mode for different NSs of masses ranging from 1.2 to $2M_\odot$. Together, there are 61 columns in each data set.

B. Sampling

We develop the GPlearn work flow, a symbolic regression algorithm, which is adept at discovering various mathematical expressions from the data set [63]. The other, like ML techniques or deep neural networks, also generate good predictive results or models but it is hard to convert the trained models into the mathematical expressions. Since we are motivated to uncover the multi-parameters relationships among different features in our datasets, the GPlearn approach is the most suitable. The FIG. 1 presents a detailed schematic diagram of a symbolic regression work flow we have employed.

To start our analysis, first we need to isolate the char-

acteristic/feature vectors, represented as $\mathbf{X}[i]$, and their respective target vectors, represented as $\mathbf{Y}[i]$, from the data sets. Moving forward, we then need to choose a random subset of features, \mathbf{n}_1 , from the original \mathbf{n} features alongside a randomly selected target from the original set. Then, these random combinations of $\mathbf{X}[\mathbf{n}']$ and $\mathbf{Y}[1]$ are passed through the GPlearn algorithm to find the best relations among them. To fine tune the hyper-parameters of the GPlearn method such as iteration count and operators, we adopt two optimization techniques: (i) *Bayesian optimization* and (ii) *a systematic grid search*. Taking advantage of both methods, we identify the optimal equation that demonstrates the minimal relative error and the strongest Pearson correlation coefficient between \mathbf{X} and \mathbf{Y} . We repeat this procedure more than N times. The number N depends on the number of combinations that are being sampled from the feature list at a time. For example, for 6 features if we pass 3 features in each iteration then the number of iterations needed are $N = {}^6C_3$.

V. RESULTS AND DISCUSSIONS

One of the primary aims of this analysis is to investigate the relationships between the non-radial oscillations particularly the f mode frequencies, various properties of NSs for various masses, and, various nuclear saturation properties. Our calculation of the f mode oscillations is restricted to the Cowling approximation [25, 61]. We use a wide range of EOS models. These models are of two distinct families based on RMF theory of nuclear matter: the first family consists of models with density-dependent coupling (DDB), and the other includes models with a constant coupling but with nonlinear mesonic interactions (NL). The distinction between these two types of models is significant as they provide different insights into the nature of nuclear forces at high-densities as in the core of NSs.

At first, we conduct a Pearson correlation analysis of the f mode frequencies and the dimensionless tidal deformabilities of NSs of different masses considering the β -equilibrated EOS, across a range of number densities pertinent to NSs. In FIG. 2 (top panel), we display the sensitivity of the f mode frequency with the pressure at different densities ranging upto 1.25 fm^{-3} . We compute the Pearson correlation coefficient between the f mode frequencies of NSs of masses from 1.4 to $2M_\odot$ and pressures over a broad range of densities for both (DDB and NL) data sets. The figure reveals that the f mode frequencies for NSs of masses of 1.4 and $1.8 M_\odot$ form a peak or show stronger correlations with the pressures at densities ranging from 1.5 to 2.5 times nuclear saturation densities in both the data sets. Although the DDB data set exhibits a higher value of correlation as compare the same with the NL data set. It may be noted that the correlation of the f mode frequency with the pressure is negative. This is expected as may be seen in Eq. (28)

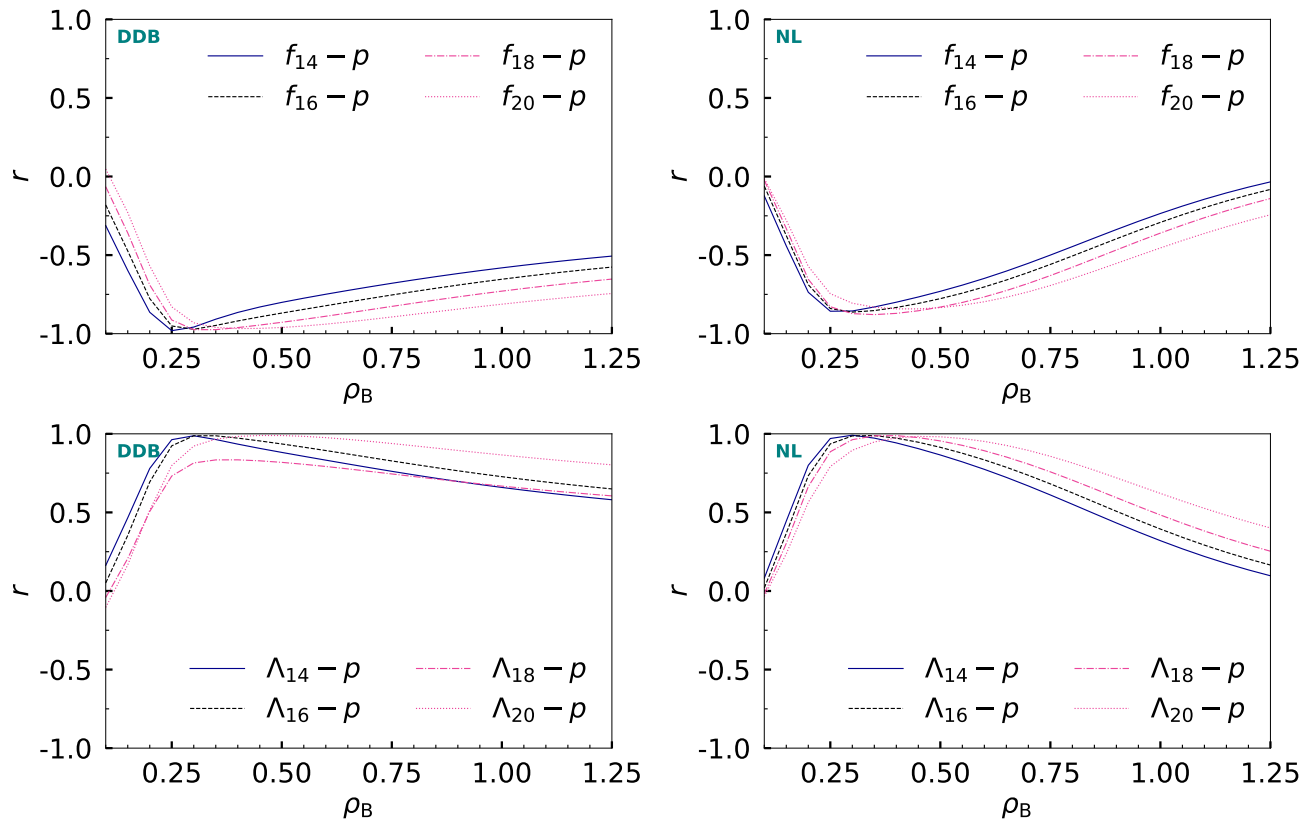


FIG. 2: In the top left and top right panels, we have the Pearson coefficient (r) of pressure with f mode frequencies for different neutron star masses in DDB and NL data, respectively. These coefficients are plotted as a function of baryon number densities. The lower panel displays a similar result for the dimensional tidal deformability.

the f mode frequency depends inversely on the square of speed of sound $\frac{dp}{d\epsilon}$ [25, 64]. It may be noted here that recent studies have consistently observed a strong correlation between f mode oscillation frequencies and EOS of NS matter [22]. For example, in Ref. [65] the authors use a selection of RMF and Skyrme EOS models to demonstrate a correlation of approximately 0.9 between the f mode frequencies for NSs of masses ranging from 1.4 to $1.8M_{\odot}$ and NS matter pressure corresponding to the densities between 1.5 to 2.5 times nuclear saturation densities. This relationship was found to be true under both the Cowling approximation and a full linearized general relativity (GR) treatment to calculate the quasi-normal mode oscillations. The Ref. [66] further supports this correlation by implementing a wide range of RMF EOS models, defined by using Bayesian inference with minimal constraints. Their results obtained with linearized GR are also consistent with the strong correlation with the NS matter pressure as previously reported [67]. These converging findings from independent studies are also true in our studies with the two different families of EOSs. In FIG. 2 (bottom panel), we present the correlation analysis of the dimensionless tidal deformability of NS of masses from 1.4 to $2M_{\odot}$ and the pressure of NS matter across densities upto 1.25 fm^{-3} . Our findings

demonstrate that the tidal deformability of NSs of masses from 1.4 to $2M_{\odot}$ are significantly impacted by EOS in the region of ~ 1.5 to 2.5 times the nuclear saturation density for both families of EOSs models. This implies that the future measurements of NS observables, such as f mode frequency and tidal deformability of NSs of 1.4 to $2M_{\odot}$ masses could be used to impose stringent constraints on EOS, particularly at higher densities. These results are consistent with the prior research outcomes derived using various EOS models, including those from the Taylor meta-modelling approach as in Ref. [68]. This consistency in findings across different EOS models and observational features strengthen that the correlations are the EOS insensitive or model independent.

We already know that the observables of NSs vary depending on their masses and are strongly correlated with the properties of nuclear matter at different densities. However, we would like to gain a deeper understanding of these correlations and investigate how they relate the different individual components of EOSs to the NS's observables. To do this, we first analyse the Pearson correlation coefficient in the DDB and NL EOSs data sets separately.

We are focus particularly on the Pearson correlation coefficients, the statistical measure that help to iden-

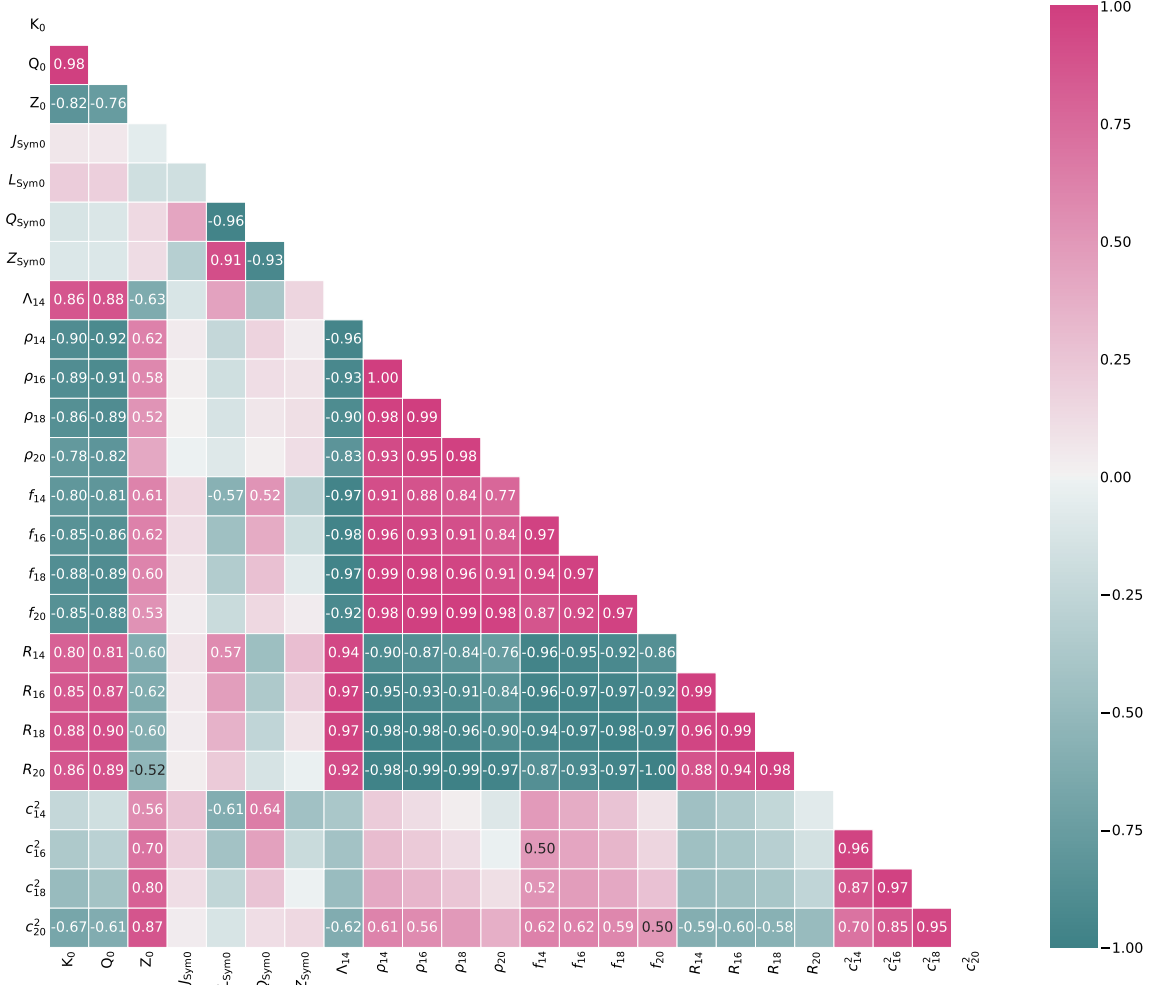


FIG. 3: The Pearson correlation coefficients with color gradient among different nuclear saturation properties calculated at saturation density ρ_0 such as incompressibility (K_0), skewness (Q_0), Kurtosis (Z_0) and slope parameter of symmetry energy (L_0), its higher order curvatures ($Q_{\text{sym},0}$, $Z_{\text{sym},0}$), tidal deformability for $1.4 M_\odot$ and various NS properties central density ($\rho_{c,m}$), radius (R_m), f mode frequency (f_m), square of speed of sound at the center of NS (c_{sm}^2), where $m \in (1.4, 1.6, 1.8, 2.0)$ (For DDB data set).

tify the strength and direction of a linear relationship between variables. In the present study, the variables include various nuclear saturation properties, NS properties, and the f mode non-radial oscillation frequencies of various NSs masses. By examining these correlations, we uncover the linear relationships between these variables. The heatmap, in FIG. 3, demonstrates the Pearson correlation coefficients between various nuclear matter properties, various properties of NSs and their f mode frequencies for the DDB dataset. It is evident that for NSs of masses ranging from 1.4 to $2M_\odot$, there is a sig-

nificant inverse relationship between the f mode frequencies and isoscalar nuclear saturation properties associated with symmetric nuclear matter. Specifically, the nuclear incompressibility (K_0) and its skewness (Q_0) have negative Pearson correlation coefficients with a magnitude exceeding 0.8 which indicates a strong anti-correlation relation. On contrary, there is no significant relationship between the isovector nuclear saturation properties associated with the symmetry energy such as symmetry energy at saturation density ($J_{\text{sym},0}$), its slope ($L_{\text{sym},0}$), its curvature ($K_{\text{sym},0}$), and, the f mode frequencies. It

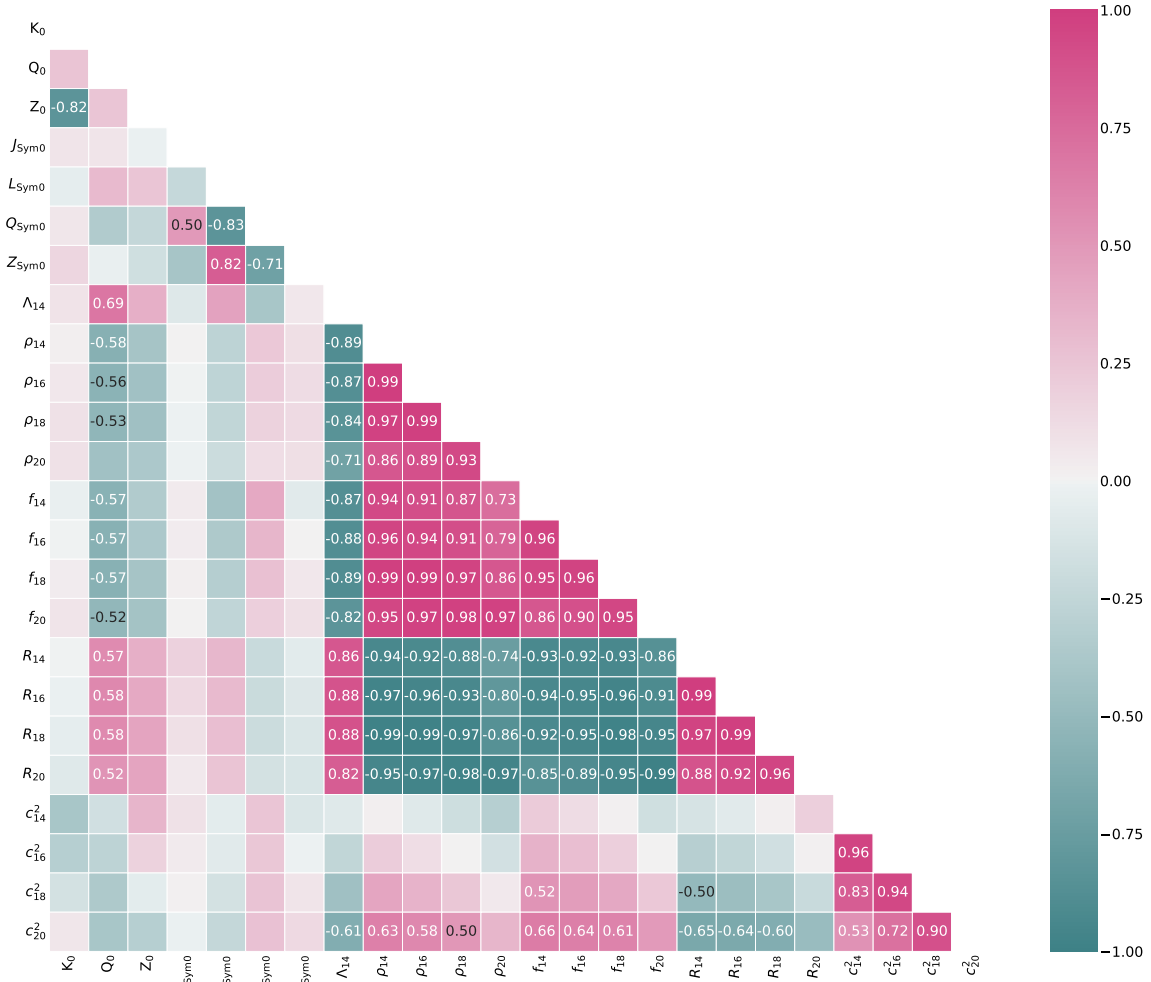


FIG. 4: The Pearson correlation coefficients as in Figure 3 but with NL type EOS.

is evident that there is a strong positive correlation with a value of coefficients over 0.9 between the f mode frequency of a given mass and its central baryon number density. This relationship is also seen with the radius of NS of the same mass implying that the f mode frequency is likely to vary in accordance with the NS's central density and radius. The different attributes of NSs like mass, radius, tidal deformability and f mode frequency with similar masses are positively correlated with each other. However, as the mass difference increases, this correlation weakens. Though it still remains strong with a value of coefficients above 0.8. Present analysis of the DDB dataset has revealed that the f mode frequencies for various NSs of masses are mainly indicative for the symmetric nuclear matter properties. In FIG. (4),

we present the same for the NL dataset. The results are strikingly different from the DDB dataset. Our findings suggest that the f mode frequencies for NSs of masses between 1.4 and $2M_{\odot}$ in the NL dataset do not show any correlation with individual nuclear saturation properties. Such an observation asserts that NS properties and nuclear saturation properties are EOS model dependent. This means that the same high density behaviour originating from different families of EOSs can lead to different nuclear saturation properties and vice-versa. This is in agreement with the results of Ref. [66] where they studied in the full GR analysis for the f mode frequencies as opposed to the Cowling approximation applied here. Additionally, there are observable correlations between the f mode frequencies and other stellar properties

such as the central baryon number densities (ρ_c) and the NS radii. These correlations remain consistent across the various NSs of different masses.

In FIG. 5, we plot the Kernel distribution estimation for the f mode frequencies (f_{20}) of NSs of mass $2M_\odot$ and the incompressibility of nuclear matter (K_0) (top left) and the skewness parameter (Q_0) (top right) at nuclear saturation densities for the DDB data set. The same estimations are shown in the bottom panel for the NL data set. From this figure, it is observed that the f_{20} exhibits a strong correlation with K_0 and Q_0 related to the symmetric nuclear matter for the DDB data set while such correlations are absent for the NL data set. This, therefore, suggests that inferring the nuclear matter properties from the f mode frequencies of NSs is rather model dependent. It is noteworthy that the correlation analysis gives us an understanding of the individual parameter relationships. A more comprehensive multi-parameter correlation analysis [28] is planned for the next stage of the present study to explore the interconnections between the properties of nuclear matter and NS observations in greater detail.

Despite our thorough examination we have not seen a clear connection between the f mode frequency and individual elements of EOS like various nuclear saturation properties in a model independent way *i.e.* a way which is consistent across both the DDB and the NL datasets. The Pearson correlation analysis is the only way to explore a relationship between two parameters. So it may miss out one or more intricate, multi-parameter interactions or nonlinear relationships that could be present. We have sought to explore the potential correlations using the DDB and NL models by utilizing ML techniques. The ML ability to identify the subtle patterns in large datasets makes it an ideal tool for the present exploration. This technique allows us to surpass the restrictions of traditional statistical methods and potentially uncover intricate connections within the datasets that have been previously undiscovered. To explore the general model independent relationships, we first combine and mix uniformly both the datasets. We then divide the whole dataset into two components or vectors: the feature vector and the target vector. In our ML framework the feature vector, denoted as \mathbf{X} , is carefully selected to encompass a range of nuclear saturation properties. These include the binding energy per baryon (\mathbf{e}_0), nuclear matter incompressibility (K_0), skewness (Q_0), kurtosis (Z_0), symmetry energy ($J_{\text{sym},0}$), its slope ($L_{\text{sym},0}$), curvature ($K_{\text{sym},0}$) as well as other higher-order coefficients like $Q_{\text{sym},0}$ and $Z_{\text{sym},0}$. The target vector, denoted as \mathbf{Y} , is chosen to be the f mode frequencies corresponding to NSs of masses ranging from 1.2 to $2M_\odot$. To probe the underlying relationships between the features and targets, we employ a symbolic regression. This method is detailed in section IV B. We apply over 150 iterations for randomly chosen sets of four feature vectors and one target vector. The symbolic regression is particularly suited for this task as it can reveal both simple

and complex mathematical relationships within the data. As mentioned in section IV B, we rank the relationships based on the minimal relative error and the best Pearson correlation coefficient. In the TABLE I, we give the best relations obtained from this search within the mixed dataset. These relations elucidate the strongest relationships discovered between the combination of nuclear saturation properties and the f mode frequencies for various NS across both the DDB and NL data sets. Notably, the most substantial correlation exhibiting a Pearson coefficient of 0.8 is found with f_{12} . The relative error margin for the equations remains within a tight 3% threshold. It is important to highlight that the relationships depicted in the table I are having dimensions. For example, the f mode frequency is measured in kHz while the saturation properties are quantified in MeV. It is also evident that among the spectrum of saturation properties, the f_{12} strongly correlates with the isoscalar component K_0 , and the isovector components $L_{\text{sym},0}$ and $K_{\text{sym},0}$, which are the indicators of symmetry energy. As we examine f_{14} , a similar pattern also emerges. The higher-order isoscalar property Q_0 begins to feature in the relationships. This meticulous symbolic regression search reveals that these parameters effectively represent the interplay between the symmetric and asymmetric components of EOS in their correlation with the f mode frequency. The parallel observations have been made concerning other NS observables such as tidal deformability which show a correlation with the nuclear matter parameters. This includes a component from EOS of symmetric nuclear matter along with the another component from EOS of asymmetric matter as detailed in the Ref. [69]. This reinforces the notion that the EOS's symmetric and asymmetric properties together play an important role in the behaviour of NS attributes.

The results of our investigation have motivated us to further explore the relative contribution of the saturation properties K_0 , Q_0 , $J_{\text{sym},0}$, and $K_{\text{sym},0}$ to the f mode oscillations of NSs with masses ranging from 1.4 to $2M_\odot$. To do this, we conduct a PCA using the combined dataset of DDB and NL models. We use the coefficients obtained from a linear fit of the f mode frequency and the four features (the saturation properties) mentioned above to obtain the contributions of different nuclear saturation properties to the f mode frequency of NSs of different masses. Through PCA analysis, we estimate the percentage of variance of each feature for each principal component.

In FIG. 6, we plot the percentage variance bars of the different features in different principal components PCA1 to PCA4 for the f modes (f_{12} , f_{14} , f_{16} , and f_{18}) of NS of masses 1.2, 1.4, 1.6 and $1.8M_\odot$ from top left to bottom right, respectively. The sky blue and orange colors represent the nuclear saturation properties pertaining the symmetric matter properties like incompressibility (K_0) and skewness (Q_0) respectively. Whereas the green and red colors are for the symmetry energy elements of nuclear matter EOS such as the slope parameter ($L_{\text{sym},0}$)

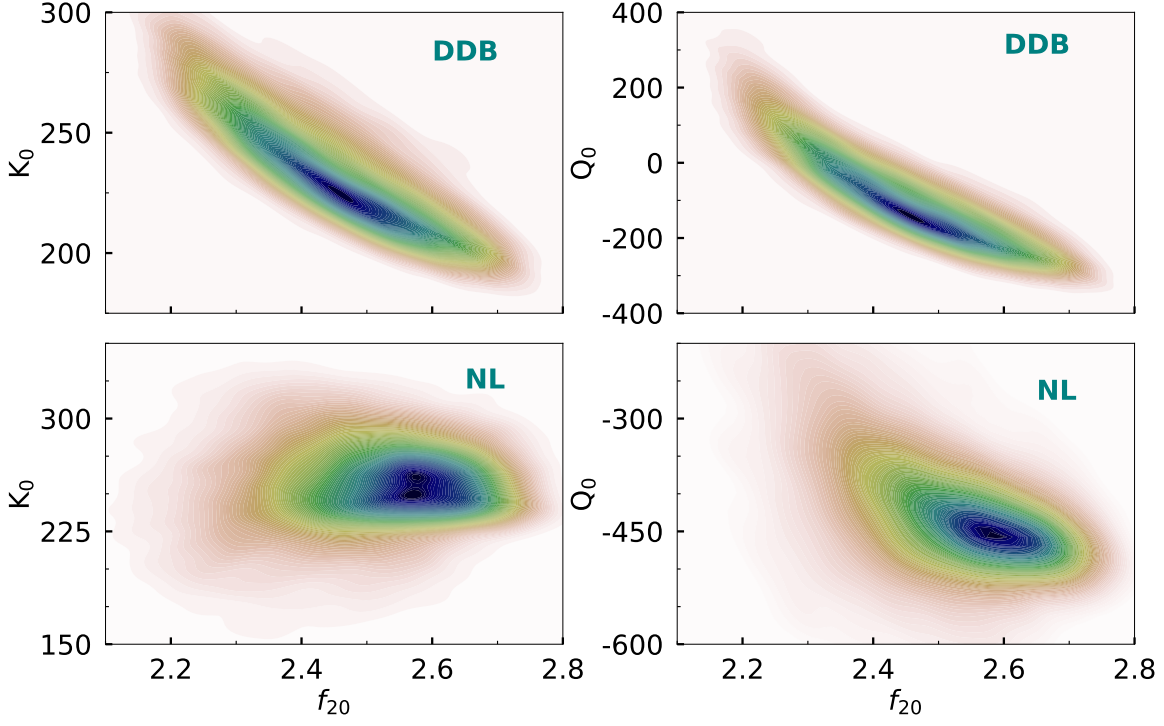


FIG. 5: The 2D distribution among incompressibility at nuclear saturation - $f_{2.0M_{\odot}}$ (top, left), skewness at nuclear saturation - $f_{2.0M_{\odot}}$ (top, right) for DDB. Same as for NL data set at (bottom, left) and (bottom, right) respectively.

TABLE I: We present a list of semi-universal relationship among various nuclear saturation properties and f mode oscillation of different NS masses that is not affected by the equation of state, which was obtained through symbolic regression on a combination of DDB and NL data sets.

y	Relationship	Corr	RE
f_{12}	$-1.48 \times 10^{-5} L_{\text{sym},0} (1.48 K_0 + K_{\text{sym},0}) + 2.31$	0.79	1.58
f_{14}	$L_{\text{sym},0} (-2.38 \times 10^{-5} K_0 - 2.10 \times 10^{-5} K_{\text{sym},0}) + 2.36$	0.77	1.7
f_{16}	$2.21 - 0.17 \frac{K_{\text{sym},0} + L_{\text{sym},0} + 0.18 Q_0}{K_0}$	0.74	1.92
f_{18}	$2.31 + \frac{L_{\text{sym},0} - Q_0}{L_{\text{sym},0} (K_0 + K_{\text{sym},0})}$	0.71	2.12
f_{20}	$-0.41 \times 10^{-3} K_{\text{sym},0} - 0.41 \times 10^{-3} Q_0 + 2.33$	0.66	3.06

and the curvature ($K_{\text{sym},0}$). In the current study, we have observed that the combination of nuclear saturation properties in the principal components varies across the NSs of different masses. For example, the f_{12} frequency (the first principal component), explaining 45% of variance, is primarily influenced by the slope of the symmetry energy $L_{\text{sym},0}$ whereas the curvature of the symmetry energy $K_{\text{sym},0}$ and the nuclear matter incompressibility, K_0 are more significant in the second and third components, explaining 28% and 20% of the variance, respectively. Moving to the f_{14} frequency (the first principal component), explaining 31% of variance, is influenced by both $K_{\text{sym},0}$ and $L_{\text{sym},0}$ where $K_{\text{sym},0}$ makes

the significant representation of 25%. The contribution of $L_{\text{sym},0}$ is dominant in the second principal component, accounting for 24% of the overall contribution. The (K_0) becomes prominent in the third component (20%). As we consider the f_{16} frequency, the analysis indicates a shift with $K_{\text{sym},0}$ becoming the most substantial factor in the first principal component (33% of variance) followed by the higher-order isoscalar property Q_0 in the second principal component (17%) and K_0 in the third principal component (20%). For the f_{18} frequency, both $K_{\text{sym},0}$ and Q_0 significantly contribute to the first and second principal components explaining 21% and 18% of the variance respectively and K_0 remains a consistent

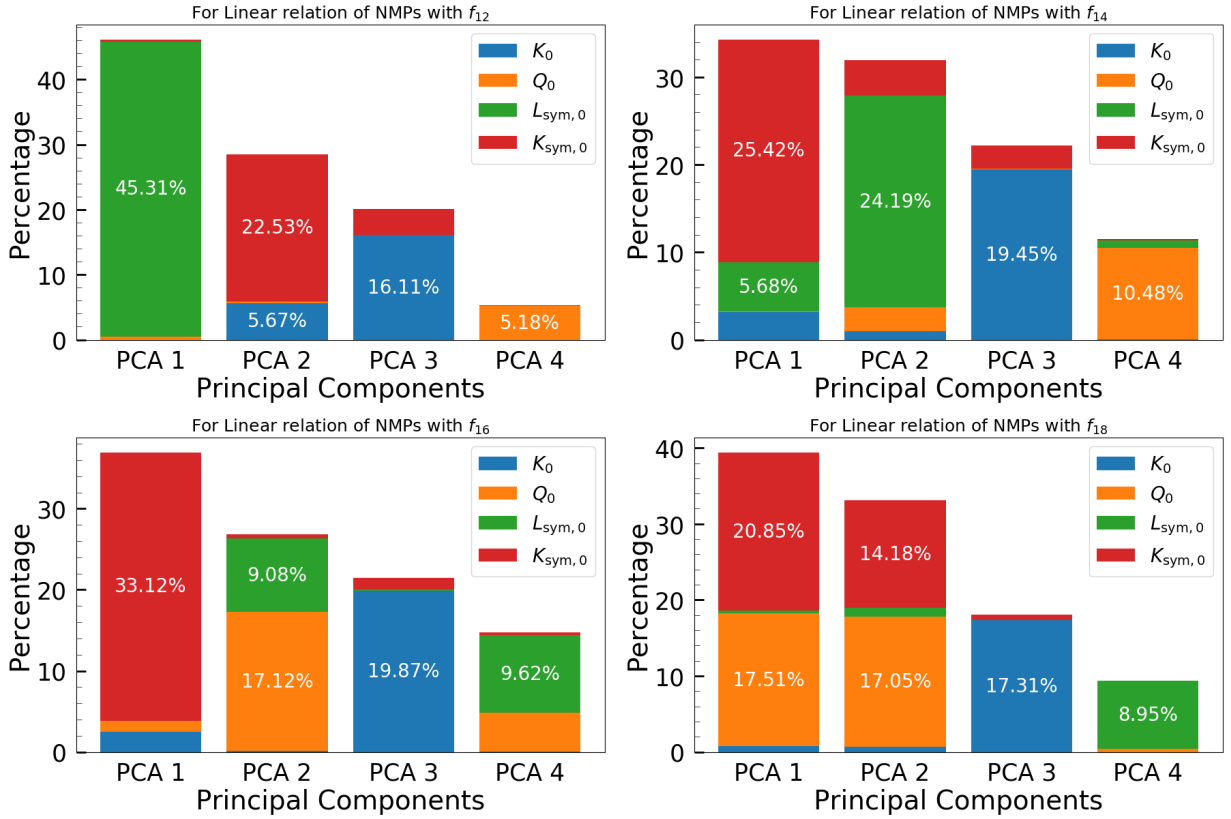


FIG. 6: The variance (expressed as a percentage) of the principal components associated with the f mode oscillations of neutron stars with masses ranging from 1.4 to 1.8 M_{\odot} is presented, along with the percentage contribution of the various NMPs to each PCA axis.

factor in the third principal component (17%). These results suggest that the f mode frequency for the lower mass NSs encapsulate substantial information about the nuclear symmetry energy as evidenced by $L_{\text{sym},0}$. The significance of higher-order symmetry energy parameters such as $K_{\text{sym},0}$, and Q_0 escalate with NSs of larger mass. Particularly for NSs of $1.8M_{\odot}$ these properties significantly influence the primary principal component. Thus we conclude that the lower mass NSs reflect the detailed information about nuclear symmetry energy in their f modes while the higher mass NSs reflect the symmetric nuclear properties.

To enhance our understanding of the model independent relevance of different nuclear saturation properties to f mode frequencies, our study also includes a feature importance analysis *i.e.* a key concept in ML. The feature importance refers to a technique that assigns a score to input features based on their usefulness in predicting a target variable. In this context, we utilize the combined dataset comprising both DDB and NL models and apply a random forest classifier in the present analysis. A random forest, an ensemble learning method, constructs multiple decision trees during the training and gives a class that is the mode of the classes of a individual tree. It gauges the importance of each feature by observing how much prediction errors increase when data for that

feature is randomly shuffled. Thus disrupting the relationship between the feature and the target. This approach allow us to assess the influence of all seven nuclear saturation properties on the f mode frequencies across a different NS of masses from 1.2 to $2M_{\odot}$. The process not only identifies which features are the most influential but also quantifies their relative importance in predicting the f mode frequency. In figure 7 we present the percentage of the feature importance of the different features *i.e.*, K_0 , Q_0 , Z_0 , $L_{\text{sym},0}$, and $K_{\text{sym},0}$ against the f mode frequencies of NSs of masses from 1.2 to $2M_{\odot}$. For the f mode frequency (f_{12}) the symmetric matter features of EOSs show a combined importance of 45% with individual contributions being 15% for K_0 , 21% for Q_0 , and 9% for Z_0 while the symmetry energy features contribute 54% divided as 36% for $L_{\text{sym},0}$ and 18% for $K_{\text{sym},0}$. Moving to f_{14} the symmetric matter features increase their combined importance to 60% with Q_0 alone accounting for 40% while the symmetry energy features contribute 39% with $L_{\text{sym},0}$ at 21%. Similarly, for f_{16} the importance of the symmetric matter features continues to increase and reaches to 71% dominated by (Q_0) at 50%. On contrary, the contribution from symmetry energy features decreases to 29%. In the case of f_{18} the trend persists, with the symmetric matter comprising 77% of feature importance and the symmetry energy features accounting

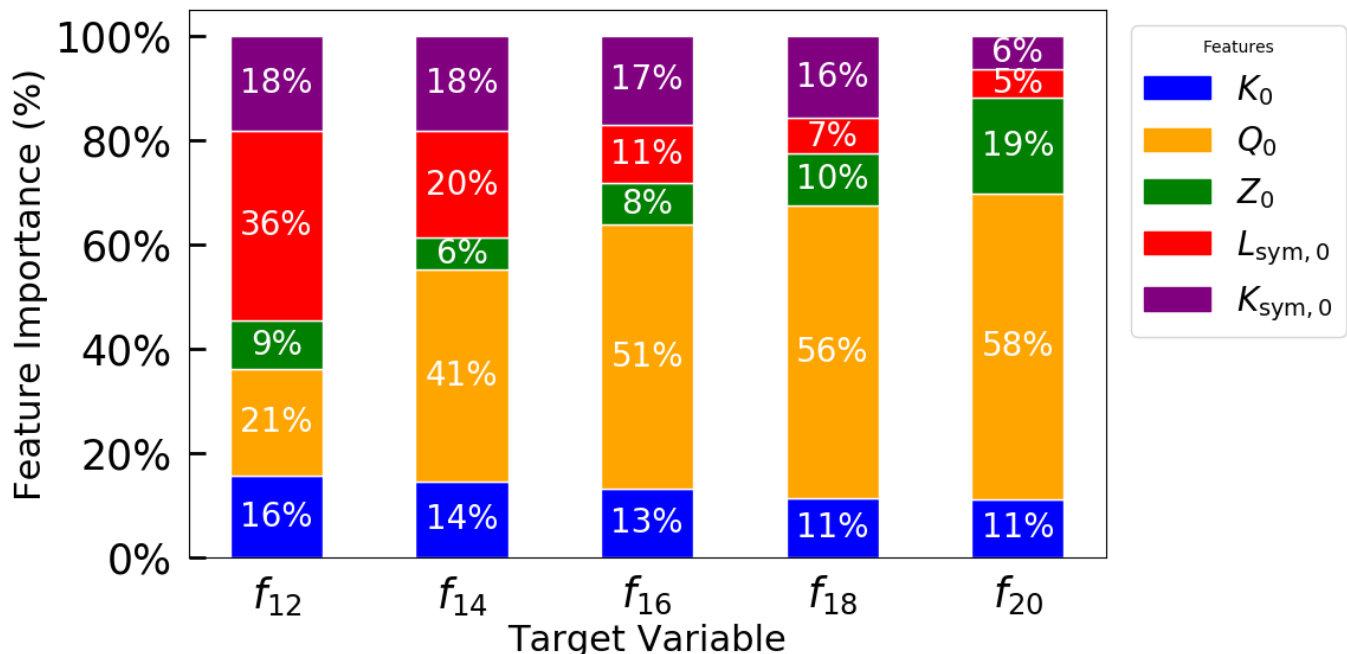


FIG. 7: The Random forest classifier with a mixed dataset of NL and DDB was used to plot the percentage of feature importance for the target as a function of the neutron star mass, which ranged from 1.2 to $2M_{\odot}$.

for 23%. Finally, for f_{20} the analysis shows a striking 88% feature importance for the symmetric matter features with a significant (58%) contribution from Q_0 alone while the symmetry energy features contribute only 11%.

This analysis aligns with the PCA results and conclusively indicates that the f mode frequency for lower mass NSs predominantly carries the imprint of the nuclear symmetry energy. While for higher mass NSs, it reflects information about the symmetric nuclear matter more significantly. For instance, the f mode of a NS of mass $2M_{\odot}$ is composed of 90% information pertaining to symmetric matter. These findings are crucial for the future observations and underline the necessity of the precise f mode measurements across a range of NSs to independently constrain both the symmetry energy and asymmetric nuclear matter components of EOS. Our analysis is the pioneering to dissect the significance of individual components of NS matter EOS in relation to f mode oscillation frequencies, employing ML techniques.

In the final phase of the present analysis, we embark on another round of symbolic regression research to look for universal relationships between the f mode frequency of NSs of various masses and a wider set of features. In addition to nuclear saturation properties, we incorporate features representing the central properties of NSs, such as baryon number density (ρ_c), pressure (p_c), energy density (ϵ_c) and the square of the speed of sound (c^2) for NSs of masses ranging from 1.4 to $2M_{\odot}$. Following the methodology outlined in section IV, we select the random combinations of four features and one

target for each Gplearn symbolic regression search and iterate the process 1,00,000 times. The most promising relations derived from this search, which boast Pearson coefficients exceeding 0.9 and remarkably low relative errors — with a maximum of 1% for a relation involving f_{20} — are presented in TABLE II. It is important to note that in these relationships, the frequency is measured in kHz, while other quantities such as energy density and pressure are expressed in MeV/fm^3 and baryon number density in fm^{-3} . The saturation properties like the symmetry energy slope parameter are in MeV and the square of the speed of sound is presented in c^2 units.

These derived relations offer a valuable predictive potential which can be used to estimate the central energy density, pressure, baryon number density, and/or the speed of sound at the center of NSs from the observed frequency of f mode oscillations in a model independent manner. This capability marks a significant advancement in our understanding of NS internal dynamics and could be pivotal in interpreting future observational data. By bridging the gap between observable oscillation frequencies and the underlying physical properties of NSs, these relations provide a powerful tool in astrophysical research.

VI. SUMMARY AND CONCLUSION

In this comprehensive study, we have explored the relationships between the non-radial f mode frequency of NSs and different saturation properties of nuclear matter

TABLE II: Universal relations between the f mode frequencies corresponding to the neutron stars of different masses ranging from 1.2 to $2M_\odot$ and different central properties of NSs, and different saturation properties of nuclear matter. The extra symbols like c_M^2 , $\rho_{c,M}$, $p_{c,M}$, and $\epsilon_{c,M}$ represent the speed of sound, baryon number density, pressure, and energy density at the center of NS of mass M . The coefficients in all universal relations have dimensions. Baryon number density, pressure, and energy density are taken in fm^{-3} , MeV/fm^3 and, MeV/fm^3 respectively

Sl No	NS mass (M_\odot)	frequency (kHz)	Universal Relationship	Corr	RE %
1	1.2	f_{12}	$0.19 + 17.65 \cdot \frac{p_{c,12}}{\epsilon_{c,12}}$	0.98	0.5
2		f_{12}	$c_{12}^2 + 2.40 - \frac{23.32}{p_{c,12}}$	0.95	0.7
3		f_{12}	$2 \cdot \rho_{c,12} - 0.002 \cdot L_{\text{sym},0} + 1.47$	0.94	0.8
4	1.4	f_{14}	$0.39 + 13.26 \cdot \frac{p_{c,14}}{\epsilon_{c,14}}$	0.98	0.5
5		f_{14}	$c_{14}^2 + 2.38 - \frac{30.51}{p_{c,14}}$	0.96	0.7
6		f_{14}	$1.74 \cdot \rho_{c,14} + c_{14}^2 + 1.08 + \frac{1.29}{L_{\text{sym},0}}$	0.97	0.6
7	1.6	f_{16}	$0.65 + 9.64 \cdot \frac{p_{c,16}}{\epsilon_{c,16}}$	0.97	0.5
8		f_{16}	$0.006 \cdot p_{c,16} + 1.77$	0.95	0.7
9		f_{16}	$1.55 \cdot \rho_{c,16} + c_{16}^2 + 1.13$	0.96	0.7
10	1.8	f_{18}	$\frac{5.69 \cdot p_{c,18}}{\epsilon_{c,18} + L_{\text{sym},0} + 236.08} + 1.53$	0.99	0.3
11		f_{18}	$0.004 \cdot p_{c,18} + 1.90$	0.97	0.6
12		f_{18}	$1.19 + \frac{0.005 \cdot p_{c,18}}{\rho_{c,18}}$	0.99	0.5
13	2.0	f_{20}	$0.84 \cdot \rho_{c,20} + 0.45 \cdot c_{20}^2 + 1.62$	0.98	0.7
14		f_{20}	$\rho_{c,20} + 1.75$	0.97	1
15		f_{20}	$0.001 \cdot p_{c,20} + 2.12$	0.96	1

within the general RMF framework for nuclear matter. Our investigation encompasses two distinct parameterizations schemes of nuclear EOS – the DDB and NL models – which align with the current understanding of nuclear matter at nuclear saturation densities and the GWs observations like tidal deformation of NSs. Our analysis reveals that the f mode frequency is intricately linked to various aspects of NS matter. The Pearson correlation coefficients from our studies indicate significant relationships between the f mode frequency, and, both symmetric and asymmetric nuclear matter properties. Notably, for lower mass NSs, the f mode frequency predominantly carries information about the nuclear symmetry energy while reflects about symmetric nuclear properties for NSs of higher masses.

The ML techniques, particularly symbolic regression, provide a novel perspective on these relationships. This approach enables us to uncover complex mathematical relationships between nuclear saturation properties and NSs of different masses which are otherwise not apparent. The PCA further reinforces these findings. It demonstrates that the composition of nuclear saturation properties significantly varies with different masses NSs. The feature importance analysis, using a mixed dataset of DDB and NL models, highlights the distinct roles of various nuclear saturation properties to determine the f mode frequency of NSs across a range of masses. This analysis is pivotal for future observations as it suggests that the precise measurements of f mode frequencies can offer insights into the EOS's symmetric and asymmetric components.

Additionally, our symbolic regression searches yield the relations with high Pearson coefficients with low relative errors, suggesting the potential avenues for predicting the central properties of NSs like central pressure, baryon number density, energy density and/or the speed of sound based on the f mode oscillation frequencies. In summary, our research not only corroborates previous studies but also extends the understanding of NS's internal dynamics. The correlations between the f mode frequencies and nuclear saturation properties revealed through various analytical and ML methods, underscore the complex nature of NSs and their potentials as cosmic laboratories for studying extreme states of matter. These insights are invaluable for future astrophysical research and could significantly impact our understanding of NS properties and behaviours.

Acknowledgments

DK would like to acknowledge the financial support from the Science and Engineering Research Board under the project no. SERB/PHY/2022-2023/68, India. T.M. would like to acknowledge the support from national funds from FCT (Fundação para a Ciência e a Tecnologia, I.P, Portugal) under projects UIDB/04564/2020 and UIDP/04564/2020, with DOI identifiers 10.54499/UIDB/04564/2020 and 10.54499/UIDP/04564/2020, respectively, and the project 2022.06460.PTDC with the associated DOI identifier 10.54499/2022.06460.PTDC. T.M. is also grateful

for the support of EURO-LABS "EUROpean Laboratories for Accelerator Based Science", which was funded by the Horizon Europe research and innovation program with grant agreement No. 101057511. The authors

acknowledge the Laboratory for Advanced Computing at the University of Coimbra for providing HPC resources that have contributed to the research results reported within this paper, URL: <https://www.uc.pt/lea>.

-
- [1] David Blaschke and Nicolas Chamel. *Phases of Dense Matter in Compact Stars*, pages 337–400. Springer International Publishing, Cham, 2018.
- [2] E. Fonseca et al. Refined Mass and Geometric Measurements of the High-mass PSR J0740+6620. *Astrophys. J. Lett.*, 915(1):L12, 2021.
- [3] Roger W. Romani, D. Kandel, Alexei V. Filippenko, Thomas G. Brink, and WeiKang Zheng. PSR J0952–0607: The Fastest and Heaviest Known Galactic Neutron Star. *Astrophys. J. Lett.*, 934(2):L17, 2022.
- [4] Thomas E. Riley et al. A *NICER* View of PSR J0030+0451: Millisecond Pulsar Parameter Estimation. *Astrophys. J. Lett.*, 887(1):L21, 2019.
- [5] M. C. Miller et al. PSR J0030+0451 Mass and Radius from *NICER* Data and Implications for the Properties of Neutron Star Matter. *Astrophys. J. Lett.*, 887(1):L24, 2019.
- [6] Thomas E. Riley et al. A *NICER* View of the Massive Pulsar PSR J0740+6620 Informed by Radio Timing and XMM-Newton Spectroscopy. *Astrophys. J. Lett.*, 918(2):L27, 2021.
- [7] M. C. Miller et al. The Radius of PSR J0740+6620 from *NICER* and XMM-Newton Data. *Astrophys. J. Lett.*, 918(2):L28, 2021.
- [8] B. P. Abbott et al. Multi-messenger Observations of a Binary Neutron Star Merger. *Astrophys. J. Lett.*, 848(2):L12, 2017.
- [9] B. P. Abbott et al. GW170817: Observation of Gravitational Waves from a Binary Neutron Star Inspiral. *Phys. Rev. Lett.*, 119(16):161101, 2017.
- [10] J. Näätä, A. W. Steiner, J. J. E. Kajava, V. F. Suleimanov, and J. Poutanen. Equation of state constraints for the cold dense matter inside neutron stars using the cooling tail method. *Astron. Astrophys.*, 591:A25, 2016.
- [11] Feryal Özel and Paulo Freire. Masses, Radii, and the Equation of State of Neutron Stars. *Ann. Rev. Astron. Astrophys.*, 54:401–440, 2016.
- [12] Andrew W. Steiner, James M. Lattimer, and Edward F. Brown. The Equation of State from Observed Masses and Radii of Neutron Stars. *Astrophys. J.*, 722:33–54, 2010.
- [13] Anna L. Watts et al. Colloquium : Measuring the neutron star equation of state using x-ray timing. *Rev. Mod. Phys.*, 88(2):021001, 2016.
- [14] Nils Andersson and Kostas D. Kokkotas. Gravitational waves and pulsating stars: What can we learn from future observations? *Phys. Rev. Lett.*, 77:4134–4137, 1996.
- [15] Alejandro Torres-Forné, Pablo Cerdá-Durán, Andrea Passamonti, and José Antonio Font. Towards asteroseismology of core-collapse supernovae with gravitational-wave observations – I. Cowling approximation. *Mon. Not. Roy. Astron. Soc.*, 474(4):5272–5286, 2018.
- [16] Alejandro Torres-Forné, Pablo Cerdá-Durán, Andrea Passamonti, Martin Obergaulinger, and José A. Font. Towards asteroseismology of core-collapse supernovae with gravitational wave observations – II. Inclusion of space–time perturbations. *Mon. Not. Roy. Astron. Soc.*, 482(3):3967–3988, 2019.
- [17] Yosuke Ashida. Multi-energy diffuse neutrino fluxes originating from core-collapse supernovae. 1 2024.
- [18] Mael Cavan-Piton, Diego Guadagnoli, Micaela Oertel, Hyeonseok Seong, and Ludovico Vittorio. Axion emission from strange matter in core-collapse SNe. 1 2024.
- [19] Hao-Sheng Wang and Kuo-Chuan Pan. The Influence of Stellar Rotation in Binary Systems on Core-Collapse Supernova Progenitors and Multi-messenger Signals. 1 2024.
- [20] Bikram Keshari Pradhan, Debarati Chatterjee, Michael Lanoye, and Prashanth Jaikumar. General relativistic treatment of f-mode oscillations of hyperonic stars. *Phys. Rev. C*, 106(1):015805, 2022.
- [21] Prashanth Jaikumar, Alexandra Semposki, Madappa Prakash, and Constantinos Constantinou. *g*-mode oscillations in hybrid stars: A tale of two sounds. *Phys. Rev. D*, 103(12):123009, 2021.
- [22] Deepak Kumar, Tuhin Malik, Hiranmaya Mishra, and Constanca Providencia. Robust universal relations in neutron star asteroseismology. *Phys. Rev. D*, 108(8):083008, 2023.
- [23] Hajime Sotani and Tomohiro Harada. Nonradial oscillations of quark stars. *Phys. Rev. D*, 68:024019, 2003.
- [24] Nils Andersson and Kostas D. Kokkotas. Towards gravitational wave asteroseismology. *Mon. Not. Roy. Astron. Soc.*, 299:1059–1068, 1998.
- [25] Deepak Kumar, Hiranmaya Mishra, and Tuhin Malik. Non-radial oscillation modes in hybrid stars: consequences of a mixed phase. *JCAP*, 02:015, 2023.
- [26] Michele Maggiore et al. Science Case for the Einstein Telescope. *JCAP*, 03:050, 2020.
- [27] N. K. Patra, Prafulla Saxena, B. K. Agrawal, and T. K. Jha. Establishing connection between neutron star properties and nuclear matter parameters through a comprehensive multivariate analysis. *Phys. Rev. D*, 108(12):123015, 2023.
- [28] Praveen Manoharan and Kostas D. Kokkotas. Finding Universal Relations using Statistical Data Analysis. 7 2023.
- [29] Shriya Soma, Horst Stöcker, and Kai Zhou. Mass and tidal parameter extraction from gravitational waves of binary neutron stars mergers using deep learning. *JCAP*, 01:009, 2024.
- [30] Valéria Carvalho, Márcio Ferreira, and Constanca Providencia. From NS observations to nuclear matter properties: a machine learning approach. 1 2024.
- [31] Elena Cuoco et al. Enhancing Gravitational-Wave Science with Machine Learning. *Mach. Learn. Sci. Tech.*, 2(1):011002, 2021.
- [32] Tim Whittaker, William E. East, Stephen R. Green, Luis Lehner, and Huan Yang. Using machine learning

- to parametrize postmerger signals from binary neutron stars. *Phys. Rev. D*, 105(12):124021, 2022.
- [33] Márcio Ferreira and Constança Providência. Constraints on high density equation of state from maximum neutron star mass. *Phys. Rev. D*, 104(6):063006, 2021.
- [34] Márcio Ferreira, Valéria Carvalho, and Constança Providência. Extracting nuclear matter properties from the neutron star matter equation of state using deep neural networks. *Phys. Rev. D*, 106(10):103023, 2022.
- [35] Valéria Carvalho, Márcio Ferreira, Tuhin Malik, and Constança Providência. Decoding neutron star observations: Revealing composition through Bayesian neural networks. *Phys. Rev. D*, 108(4):043031, 2023.
- [36] Isaac Vidana. Machine learning light hypernuclei. *Nucl. Phys. A*, 1032:122625, 2023.
- [37] Shriya Soma, Lingxiao Wang, Shuzhe Shi, Horst Stöcker, and Kai Zhou. Neural network reconstruction of the dense matter equation of state from neutron star observables. *JCAP*, 08:071, 2022.
- [38] Nour Makke and Sanjay Chawla. Interpretable scientific discovery with symbolic regression: A review, 2023.
- [39] Sheng Sun, Runhai Ouyang, Bochao Zhang, and Tong-Yi Zhang. Data-driven discovery of formulas by symbolic regression. *MRS Bulletin*, 44(7):559–564, 2019.
- [40] J. D. Walecka. A Theory of highly condensed matter. *Annals Phys.*, 83:491–529, 1974.
- [41] J. Boguta and A. R. Bodmer. Relativistic Calculation of Nuclear Matter and the Nuclear Surface. *Nucl. Phys.*, A292:413–428, 1977.
- [42] J. Boguta and Horst Stoecker. Systematics of Nuclear Matter Properties in a Nonlinear Relativistic Field Theory. *Phys. Lett.*, 120B:289–293, 1983.
- [43] Brian D. Serot and John Dirk Walecka. Recent progress in quantum hydrodynamics. *Int. J. Mod. Phys.*, E6:515–631, 1997.
- [44] Amruta Mishra, P. K. Panda, and W. Greiner. Vacuum polarization effects in hyperon rich dense matter: A Non-perturbative treatment. *J. Phys. G*, 28:67–83, 2002.
- [45] Laura Tolos, Mario Centelles, and Angels Ramos. Equation of State for Nucleonic and Hyperonic Neutron Stars with Mass and Radius Constraints. *Astrophys. J.*, 834(1):3, 2017.
- [46] B. P. Abbott et al. GW170817: Measurements of neutron star radii and equation of state. *Phys. Rev. Lett.*, 121(16):161101, 2018.
- [47] S. Typel and H. H. Wolter. Relativistic mean field calculations with density dependent meson nucleon coupling. *Nucl. Phys. A*, 656:331–364, 1999.
- [48] B. K. Agrawal, Tuhin Malik, J. N. De, and S. K. Samad-dar. Constraining nuclear matter parameters from correlation systematics: a mean-field perspective. *Eur. Phys. J. ST*, 230(2):517–542, 2021.
- [49] Tuhin Malik, Márcio Ferreira, B. K. Agrawal, and Constança Providência. Relativistic Description of Dense Matter Equation of State and Compatibility with Neutron Star Observables: A Bayesian Approach. *Astrophys. J.*, 930(1):17, 2022.
- [50] Jia Zhou, Jun Xu, and Panagiota Papakonstantinou. Bayesian inference of neutron-star observables based on effective nuclear interactions. *Phys. Rev. C*, 107(5):055803, 2023.
- [51] Bhaskar Biswas, Evangelos Smyrniotis, Ioannis Liodis, and Nikolaos Stergioulas. A Bayesian investigation of the neutron star equation-of-state vs. gravity degeneracy. 9 2023.
- [52] Massimo Vaglio, Costantino Pacilio, Andrea Maselli, and Paolo Pani. Bayesian parameter estimation on boson-star binary signals with a coherent inspiral template and spin-dependent quadrupolar corrections. *Phys. Rev. D*, 108(2):023021, 2023.
- [53] Zhenyu Zhu, Ang Li, and Tong Liu. A Bayesian Inference of a Relativistic Mean-field Model of Neutron Star Matter from Observations of NICER and GW170817/AT2017gfo. *Astrophys. J.*, 943(2):163, 2023.
- [54] S. Wesolowski, N. Klco, R. J. Furnstahl, D. R. Phillips, and A. Thapaliya. Bayesian parameter estimation for effective field theories. *J. Phys. G*, 43(7):074001, 2016.
- [55] R. J. Furnstahl, N. Klco, D. R. Phillips, and S. Wesolowski. Quantifying truncation errors in effective field theory. *Phys. Rev. C*, 92(2):024005, 2015.
- [56] Gregory Ashton, Eric Thrane, and Rory J. E. Smith. Gravitational wave detection without boot straps: a Bayesian approach. *Phys. Rev. D*, 100(12):123018, 2019.
- [57] Philippe Landry, Reed Essick, and Katerina Chatziioannou. Nonparametric constraints on neutron star matter with existing and upcoming gravitational wave and pulsar observations. *Phys. Rev. D*, 101(12):123007, 2020.
- [58] Tuhin Malik, Márcio Ferreira, Milena Bastos Albino, and Constança Providência. Spanning the full range of neutron star properties within a microscopic description. *Phys. Rev. D*, 107(10):103018, 2023.
- [59] N. K. Glendenning. *Compact stars: Nuclear physics, particle physics, and general relativity*. 1997.
- [60] Pablo Gregorian. Nonradial neutron star oscillations. *A Master Thesis*, pages Universiteit Utrecht, Institute for theoretical physics, November 2014.
- [61] Hajime Sotani, Nobutoshi Yasutake, Toshiki Maruyama, and Toshitaka Tatsumi. Signatures of hadron-quark mixed phase in gravitational waves. *Phys. Rev. D*, 83:024014, 2011.
- [62] P. N. McDermott, H. M. van Horn, and J. F. Scholl. Non-radial g-mode oscillations of warm neutron stars. *ApJ*, 268:837–848, May 1983.
- [63] Trevor Stephens. gplearn: Genetic programming in python. <https://github.com/trevorstevens/gplearn>, 2023.
- [64] Andreas Reisenegger and Peter Goldreich. Excitation of Neutron Star Normal Modes during Binary Inspiral. *ApJ*, 426:688, May 1994.
- [65] Athul Kunjipurayil, Tianqi Zhao, Bharat Kumar, Bijay K. Agrawal, and Madappa Prakash. Impact of the equation of state on f- and p- mode oscillations of neutron stars. *Phys. Rev. D*, 106(6):063005, 2022.
- [66] Debanjan Guha Roy, Tuhin Malik, Swastik Bhattacharya, and Sarmistha Banik. Analysis of Neutron Star f-mode Oscillations in General Relativity with Spectral Representation of Nuclear Equations of State. 12 2023.
- [67] Bikram Keshari Pradhan, Dhruv Pathak, and Debarati Chatterjee. Constraining Nuclear Parameters Using Gravitational Waves from f-mode Oscillations in Neutron Stars. *Astrophys. J.*, 956(1):38, 2023.
- [68] Márcio Ferreira, M. Fortin, Tuhin Malik, B. K. Agrawal, and Constança Providência. Empirical constraints on the high-density equation of state from multimessenger observables. *Phys. Rev. D*, 101(4):043021, 2020.
- [69] Tuhin Malik, N. Alam, M. Fortin, C. Providência, B. K. Agrawal, T. K. Jha, Bharat Kumar, and S. K. Patra. GW170817: constraining the nuclear matter equation of

state from the neutron star tidal deformability. *Phys. Rev. C*, 98(3):035804, 2018.